

## **Titania Aerogels as a Superior Mesoporous Structure for Photoanodes of Dye-Sensitized Solar Cells**

*Yi-Chun Chiang, Wei-Yun Cheng and Shih-Yuan Lu\**

Department of Chemical Engineering, National Tsing Hua University, Hsinchu, 30013, Taiwan, R.O.C.

\*E-mail: [sylu@mx.nthu.edu.tw](mailto:sylu@mx.nthu.edu.tw)

*Received: 28 May 2012 / Accepted: 11 July 2012 / Published: 1 August 2012*

---

Titania aerogels, because of their structural advantages of high porosities, high specific surface areas and three-dimensionally well-connected through pore structure, are demonstrated an excellent mesoporous structure for photoanodes of dye-sensitized solar cells. A power conversion efficiency improvement of 16% (7.22 vs. 8.36%) is achieved as compared with a P25 TiO<sub>2</sub> based cell. The structural advantages of titania aerogels in serving the functionalities of the photoanode are manifested with a smaller effective back electron transfer rate constant, 9.6 vs. 13.1 s<sup>-1</sup>, a higher steady-state conduction band electron density, 32% more, and a longer electron life time, 398 vs. 199 ms, of the photoanode as compared with that of the P25 TiO<sub>2</sub> based one.

---

**Keywords:** dye-sensitized solar cell, titania, aerogel, photoanode, mesoporous

### **1. INTRODUCTION**

Aerogels are a class of mesoporous materials possessing high specific surface areas, high porosities, and three-dimensionally (3D) well-connected through pore structure [1]. These structural features favor aerogels for applications requiring high porosities such as thermal insulations, low dielectric constant films, and low refractive index glass, in which air, the dominant constituent of the structure, provides the necessary functionalities, and for applications that involve heterogeneous interactions/reactions/charge transfers at solid-liquid interfaces such as photoanodes of dye-sensitized solar cells (DSSC), photocatalytic water splitting, electrodes for energy storage and general electrochemical processes, photocatalysis, to name just a few [2-10]. For the heterogeneous processes to proceed efficiently, large surface areas to provide abundant active sites for the interfacial events, high porosities and through pore structure to enable fast mass transfer of the liquid species to access the active sites, and 3D well-connected network to offer continuous charge transport passageways, are

desirable. Evidently, aerogels are well suited for the above mentioned applications.

DSSCs, because of their excellent performance to cost ratios, remain as one of the promising alternative clean energy harvesting technologies and continue to draw a great deal of research attention [11-20]. The photoanode of a DSSC, composed of a mesoporous semiconductor film cast on top of a transparent conductive glass and sensitized with light-absorbing dyes, is responsible for absorption and conversion of incoming photons to electrons and for transport and collection of photo-induced electrons. To effectively fulfill its designed functionalities, the following structural characteristics are favorable for photoanodes, including large surface areas to acquire high dye loadings and subsequent generation of photo-induced electrons, high porosities and through pore structure to enable easy penetration and adsorption of the dye molecules onto the semiconductor surfaces and fast mass transfer of electrolyte ions in and out of the mesoporous structure, and 3D well-connected network for delocalized charge transport to lessen the unwanted back electron transfer reactions. Evidently, these structural characteristics can be readily offered by titania aerogels.

Conventionally, the photoanodes are fabricated by casting a paste of titania nanocrystals onto a transparent conductive glass. The required mesoporous structure is formed after a suitable thermal treatment. In this article, TiO<sub>2</sub> aerogels were demonstrated a superior mesoporous structure as compared with a commercial titania nanocrystal product, P25 TiO<sub>2</sub> nanoparticles, for photoanode fabrication, achieving a significant improvement in power conversion efficiencies. Note that P25 TiO<sub>2</sub> nanoparticles are often chosen as a comparison basis for functional performances in areas such as photoanodes of DSSCs, photocatalytic water splitting, and photocatalysis, since they are commercially available and offer decent performances in these applications. Piertron et al. investigated the potential of titania aerogels as a photoanode material by measuring the incident photon to charge carrier efficiency (IPCE) of a TiCl<sub>4</sub>-treated and dye-adsorbed titania aerogel of 30 μm thick [21]. The IPCE values reached 85% in the wavelength region of 500-600 nm, indicating an excellent potential for photoanode applications. Piertron et al. however did not proceed further to assemble and investigate the performance of the cells. Sung et al. spin-coated titania wet gels onto fluorine-doped tin oxide glass to serve as the photoanode of their DSSCs after drying with a supercritical fluid and obtained a power conversion efficiency of 3.71% [22]. The drawback of their approach lies in the difficulties of producing thick enough titania aerogel layers to ensure enough dye-loading and in the long aging time of several weeks needed to stabilize the aerogel structure on the FTO glass.

In this work, titania aerogel powders of high specific surface areas and pore volumes and suitable pore sizes were synthesized and used to fabricate photoanodes for DSSC study. The performance of the titania aerogel based DSSC was demonstrated superior than the P25 TiO<sub>2</sub> based DSSC, with a power conversion efficiency improvement of 16% (7.22 vs. 8.36%). The structural advantages of titania aerogels in serving the functionalities of the photoanode are manifested with a smaller effective back electron transfer rate constant, 9.6 vs. 13.1 s<sup>-1</sup>, a higher steady-state conduction band electron density, 32% more, and a longer electron life time, 398 vs. 199 ms, of the photoanode as compared with that of the P25 TiO<sub>2</sub> based one.

## 2. EXPERIMENTAL

### 2.1. Preparation of TiO<sub>2</sub> aerogels.

The TiO<sub>2</sub> aerogels were prepared following the procedures of Dagan and Tomkiewicz with minor modifications [23]. Typically, 3.025 mL titanium tetrakisopropanolate (TTIP, 97%, Aldrich), the precursor of the TiO<sub>2</sub>, was dissolved in 2.575 mL ethanol and the mixture was stirred for 1 hr. An acidic catalyst, prepared by mixing 0.0554 mL HNO<sub>3</sub>, 7.715 mL ethanol, and 0.34 mL deionized (DI) water, was added to the TTIP solution to obtain the TiO<sub>2</sub> sol. The sol gelled in one day, and the wet gel was aged for four days before being dried with the supercritical carbon dioxide to afford the highly porous TiO<sub>2</sub> aerogel. The product aerogel was calcined at 500 °C for 10 hr to acquire the preferred crystalline anatase phase.

### 2.2. Preparation of photoanodes.

The photoanode was fabricated by casting a layer of TiO<sub>2</sub> paste (aerogel or P25) of suitable thicknesses onto a fluorine doped tin oxide (FTO) glass with the doctor-blade method. The pastes were prepared by mixing 0.15 g aerogels or P25 powders with a binder solution composed of 0.025 g ethyl cellulose (200 cps, Showa) and 1 ml  $\alpha$ -terpineol (95%, Showa). The as-fabricated photoanodes were calcined at 500 °C for 30 minutes to remove the residual solvent and binder, and also to enhance the adhesion between the aerogels or P25 powders and the FTO glass. For the TiCl<sub>4</sub> treatment, the photoanode was immersed into a 0.2 M ethanolic solution of TiCl<sub>4</sub> at 80 °C for 1 hr followed by rinsing with DI water to form TiO<sub>2</sub> nanoparticles on the surface of the primitive TiO<sub>2</sub> nanostructure. The product was further calcined at 500 °C for 2 hr to acquire the crystallinity of the newly-generated TiO<sub>2</sub> nanoparticles.

### 2.3. Fabrication of dye sensitized solar cells.

The photoanodes with a working area of 0.25 cm<sup>2</sup> were soaked in a 0.3 mM *cis*-bis(isothiocyanato)bis(2,2'-bipyridi-4,4'-dicarboxylatoruthenium(II)bis-tetrabutylammonium (N719, Solaronix) solution for 12 hr for dye adsorption. Here the solvent for the N719 dye was composed of ethanol and acetonitrile at a volume ratio of 1:1. As for the electrolyte, acetonitrile was used as the solvent and the electrolyte contained 0.6M 1-propyl-2, 3-dimethylimidazolium iodide (99%, Aldrich), 0.1 M LiI (99.9%, Aldrich), 0.05M I<sub>2</sub> (99.5%, Fluka), and 0.5 M *tert*-butyl pyridine (98%, Fluka). A 100 nm thick Pt film was deposited onto an FTO glass with sputtering to serve as the counter electrode for the cell. To fabricate the cell, a spacer with a thickness of 25 micrometers was used to connect the counter electrode and photoanode.

### 2.4. Characterizations.

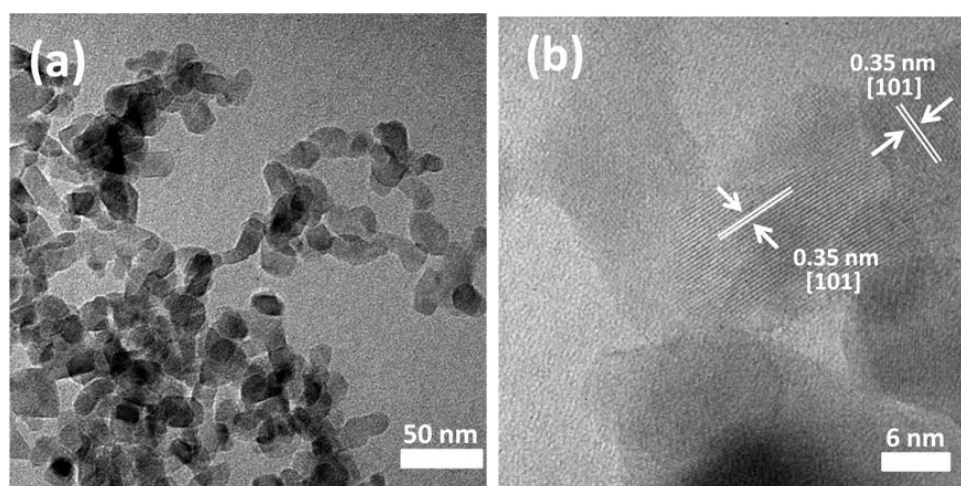
An X-ray powder diffractometer (XRD, MAC Science MXP 18) is used to determine the crystalline phase, grain size and phase purity of the TiO<sub>2</sub> samples. The morphology and

crystallographic structure of the  $\text{TiO}_2$  aerogels are investigated with a high-resolution transmission electron microscope (HRTEM, JEOL JEM-4000EX). The microstructural characteristics of the samples are measured with the  $\text{N}_2$  adsorption/desorption analyses conducted at 77 K (Quantachrome, NOVA e1000). The current density-voltage (J-V) curves of the cells were recorded with a source meter (Kiethley 236, Kiethley) under illumination of a solar simulator (Yamashita Denso, YSS-E40; AM 1.5,  $100 \text{ mW cm}^{-2}$ ) calibrated by a reference Si solar cell (SN2008-152, Yamashita). The incident photon to charge carrier efficiency (IPCE, ENLI, EQE-D-3011), electrochemical impedance spectroscopy (EIS, AUTOLAB PGSTAT30), and intensity-modulated photovoltage spectroscopy (IMVS, AUTOLAB PGSTAT30) were conducted to analyze the charge transport characteristics within the photoanodes. For the EIS, the cell was illuminated under AM1.5 simulated sunlight at the open circuit voltage, and scanned with an alternative current of frequencies of 0.01- $10^6$  Hz and an amplitude of 10 mV. IMVS was conducted using a blue light diode laser ( $\lambda=470 \text{ nm}$ ) as the light source, which was driven by a Dyload interface that is connected to an AUTOLAB instrument (PGSTAT30) as the frequency response analyzer.

### 3. RESULTS AND DISCUSSION

#### 3.1. Characterizations of $\text{TiO}_2$ aerogels.

Figure 1(a) shows the TEM image of the product  $\text{TiO}_2$  aerogel after calcination, from which the mesoporous through pore structure composed of well-connected  $\text{TiO}_2$  nanocrystals is evident [8]. Such a 3D well-connected through pore structure provides a continuous charge transport network good for the photo-induced electrons to diffuse across the photoanode layer. The constituent nanocrystals of the  $\text{TiO}_2$  aerogel are with a size of around 15 nm, which is shown later to offer a large specific surface area advantageous for dye-loading of the photoanode. Figure 1(b) shows an HRTEM image of the  $\text{TiO}_2$  aerogel. It can be observed that the aerogel backbone is constructed from chemically bonded, well-connected nanocrystals.



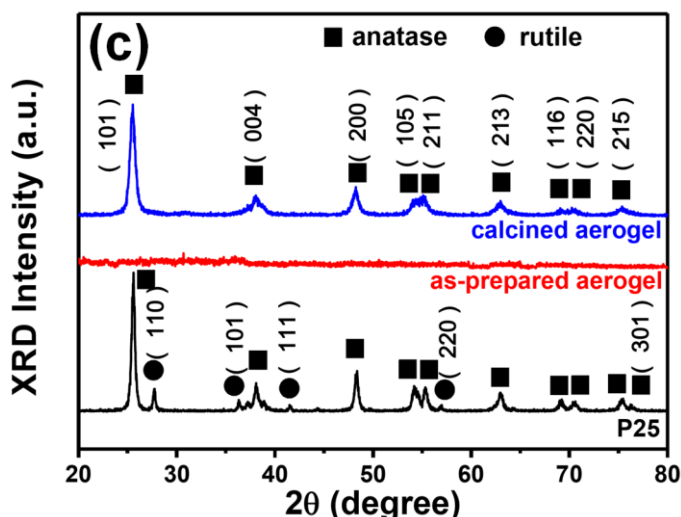


**Figure 1.** (a) TEM and (b) HRTEM images of calcined  $\text{TiO}_2$  aerogels. (c) XRD patterns of P25 and as-prepared and calcined  $\text{TiO}_2$  aerogels.

The interlayer spacing of 0.35 nm as determined from the lattice fringes is in good agreement with the  $d$ -spacing of the (101) planes of the anatase  $\text{TiO}_2$ . Figure 1(c) shows the XRD patterns of the P25  $\text{TiO}_2$  powders, as-prepared  $\text{TiO}_2$  aerogels, and calcined  $\text{TiO}_2$  aerogels. Evidently, the as-prepared  $\text{TiO}_2$  aerogels are amorphous and calcination is needed to acquire the preferred anatase phase. As for the P25  $\text{TiO}_2$ , it contains both anatase and rutile constituents as specified in its product specifications. The grain sizes of the calcined  $\text{TiO}_2$  aerogels and P25  $\text{TiO}_2$  were estimated with the Scherrer equation based on the full width at half maximum of the (101) peak to be 13.6 and 20.4 nm, respectively. Here, the closeness in the grain size and particle size (13.6 vs. 15 nm) of the constituent nanocrystals of the aerogel implies the single-crystallinity of these nanocrystals [8], which is beneficial for charge transport within the photoanode.

Further microstructural characteristics, including specific surface areas, pore volumes, and average pore sizes, of the aerogels and P25  $\text{TiO}_2$  powders were investigated with the  $\text{N}_2$  adsorption/desorption isotherms (plot not shown), and were summarized in Table 1 for comparison. Two points can be made from these data. First, smaller constituent nanocrystal sizes led to larger specific surface areas for the aerogel, which is advantageous for the subsequent dye-loading. Second, the  $\text{TiO}_2$  aerogel possessed a larger pore volume and average pore size, both are beneficial for mass transport of dye molecules and electrolyte ions within the mesoporous structure.

**Table 1.** Structural and charge transport parameters of P25 and aerogel-based photoanodes.

	specific surface area ( $\text{m}^2 \text{g}^{-1}$ )	pore volume ( $\text{cm}^3 \text{g}^{-1}$ )	avg. pore size (nm)	grain size (nm)	$D_{\text{eff}} * 10^4$ ( $\text{cm}^2 \text{s}^{-1}$ )	$k_{\text{eff}}$ ( $\text{s}^{-1}$ )	electron life time (ms)
P25	49	0.13	6	20.4	1.0	13.1	199
Aerogel	112	0.65	18	13.6	0.62	9.6	398

## 3.2. Performances of corresponding DSSCs.

The performances of the aerogel- and P25 TiO<sub>2</sub>-based cells were investigated and compared in terms of four key parameters of DSSCs. Fig. 2 shows the short circuit current density ( $J_{sc}$ ), open circuit voltage ( $V_{oc}$ ), fill factor (FF), and power conversion efficiency ( $\eta$ ) versus the photoanode thickness plots for both types of cells. The trends of  $J_{sc}$  and  $\eta$  resembled each other since  $\eta$  ( $\sim J_{sc}V_{oc}FF$ ) [11] is directly proportional to  $J_{sc}$  and  $J_{sc}$  often plays a more dominant role among the three contributing factors. Interestingly, the highest  $\eta$  for the aerogel-based cell was achieved at a larger thickness of around 16  $\mu\text{m}$ , than that of around 12  $\mu\text{m}$  for the P25-based cell. This may be attributed to the more open structure of the aerogel allowing deeper utilization lengths of the incoming light, and the better connected 3D network for charge transport enabling longer charge travel distances before the charges being trapped or consumed. In addition, the aerogel-based cells consistently outperformed the P25-based ones for  $J_{sc}$  and  $\eta$  (Figs. 2(a) & (b)) over the entire thickness range, demonstrating the superiority of TiO<sub>2</sub> aerogels over P25 TiO<sub>2</sub> as the photoanode material. The enhancement in  $J_{sc}$  was mainly contributed by the increased dye-loading (e.g.,  $0.98 \times 10^{-7}$  vs.  $1.47 \times 10^{-7}$  mol cm<sup>-2</sup> at a thickness of 12  $\mu\text{m}$ ) because of the larger specific surface area of the TiO<sub>2</sub> aerogel, and led to the corresponding boost in  $\eta$ . The  $V_{oc}$  of the two types of cells decreased with increasing thicknesses (Fig. 2(c)). This phenomenon may be understood as follows.

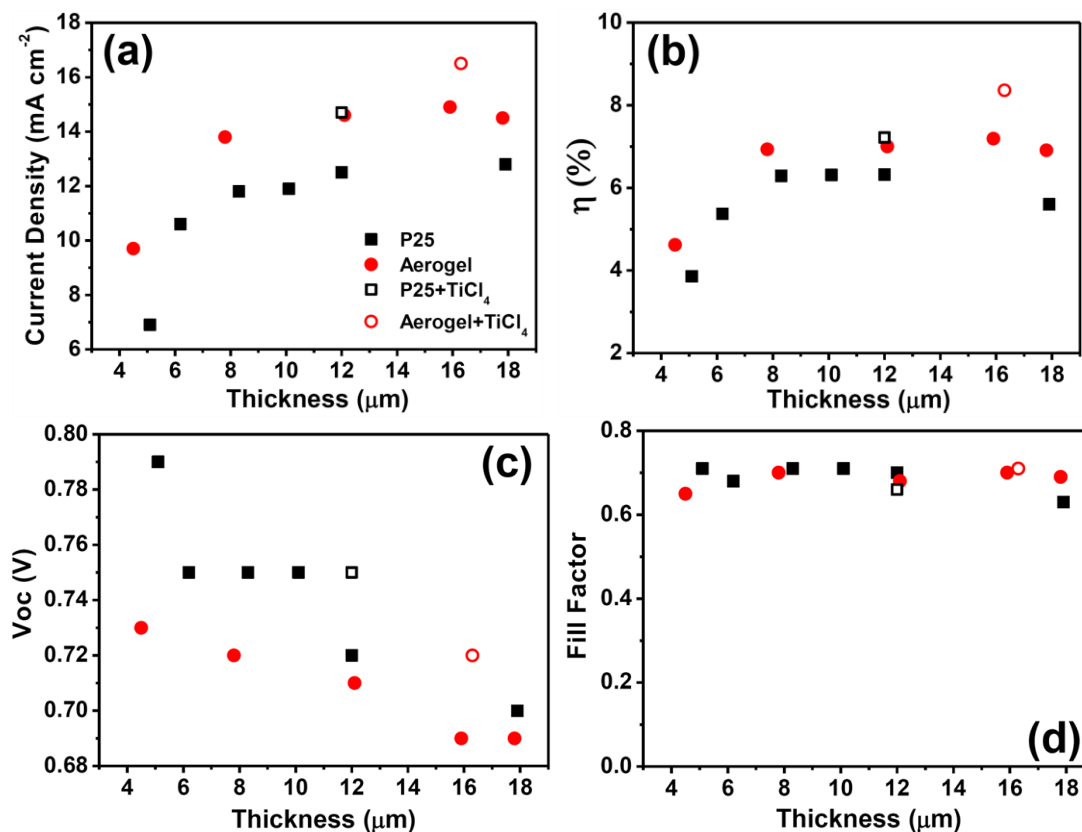


**Figure 2.** (a) Current density, (b) power conversion efficiency, (c) open circuit voltage, and (d) fill factor of aerogel and P25 TiO<sub>2</sub>-based cells as functions of photoanode thickness.

Thicker films are with longer average electron travel distances to the current collector, which in turn increase the possibility of back electron transfer during the diffusion of electrons across the film. Consequently, the electron density in the TiO<sub>2</sub> domain drops, leading to lower Fermi levels of the TiO<sub>2</sub> and thus shrinking the gap between the TiO<sub>2</sub> Fermi level and the redox potential of the electrolyte (the V<sub>oc</sub>) [24]. The FF however remained relatively unchanged (Fig. 2(d)) over the whole thickness range. The higher V<sub>oc</sub> acquired by the P25-based cells may be attributed to the denser structure of P25 aggregates on top of the FTO for better blocking ability to prevent back electron transfer at the FTO-electrolyte interface [25].

The treatment of TiCl<sub>4</sub> on the photoanode led to improved J<sub>sc</sub>, V<sub>oc</sub>, and thus η for both types of cells as evident from Figs. 2(a), (c), and (b), in which the TiCl<sub>4</sub> treated cases were designated as the corresponding open symbols at the optimum thicknesses. The treatment generated even smaller sized TiO<sub>2</sub> nanocrystals within the photoanode to offer extra surface areas for dye-loading to generate more photoinduced electrons, to improve connectivity between constituent TiO<sub>2</sub> nanocrystals for better charge transport passageways, and to form a better blocking layer on top of the FTO to further lessen the undesired back electron transfer reactions. With the TiCl<sub>4</sub> treatment, the highest η achieved by the TiO<sub>2</sub> aerogel-based cells was 8.36%, representing a 16% improvement in η over the highest η of the P25-based cells of 7.22%.

Figure 3(a) shows the J-V curves for the two types of cells at their optimum thicknesses with and without the TiCl<sub>4</sub> treatment. Evidently, the TiCl<sub>4</sub> treatment significantly increased the J<sub>sc</sub> and V<sub>oc</sub> of the corresponding cells. Figure 3(b) shows the Nyquist plots of the four cells derived from the electrochemical impedance spectroscopy. Evidently, the third arcs corresponding to the Nernst diffusion resistance of the electrolyte within the cell were absent, which was a direct result of the negligible mass transfer resistance made possible by the narrow gap of 25 μm between the anode and cathode and the use of the low viscosity electrolyte [26]. The second arc represents the impedances associated with the TiO<sub>2</sub> photoanode. The charge transport resistance of electron diffusion across the TiO<sub>2</sub> layer and the back electron transfer reactions occurring at the TiO<sub>2</sub>/dye/electrolyte interface are the two main contributors to the second arc. Following the procedures detailed in Adachi et al. [26], one can estimate values of important system parameters, such as effective electron diffusion coefficients, D<sub>eff</sub>, effective back electron transfer rate constants, k<sub>eff</sub>, and steady state electron densities in the conduction band, n<sub>s</sub>, from the Nyquist plot. To achieve high power conversion efficiencies, high D<sub>eff</sub>, low k<sub>eff</sub>, and high n<sub>s</sub> are desirable. The results for D<sub>eff</sub> and k<sub>eff</sub> for the aerogel- and P25 TiO<sub>2</sub>-based cells were included in Table 1. Both D<sub>eff</sub> and k<sub>eff</sub> of the P25 TiO<sub>2</sub>-based cell were larger than those of the aerogel-based cell, meaning electrons in the photoanode of the P25 TiO<sub>2</sub>-based cell diffused faster but also were more readily lost through the back electron transfer reactions. Nevertheless, the n<sub>s</sub> of the aerogel-based cell was 32% higher than that of the P25 TiO<sub>2</sub>-based cell, and the overall effect was a higher power conversion efficiency for the aerogel-based cell. The de-localization of electrons was enhanced in the TiO<sub>2</sub> aerogel because of its 3D well-connected structure [8]. Better electron de-localization is good to lessen back electron transfer reactions, but also tend to keep electrons wandering around isotropically instead of aiming for specific target directions to increase D<sub>eff</sub>. Nevertheless, upon the TiCl<sub>4</sub> treatment, the D<sub>eff</sub> of the aerogel-based was drastically improved to a much larger value of 1.7x10<sup>-4</sup>, even higher than 1.1x10<sup>-4</sup> cm<sup>2</sup> s<sup>-1</sup> of the P25 TiO<sub>2</sub>-based cell. The n<sub>s</sub> of

both the  $\text{TiCl}_4$  treated photoanodes were significantly increased to be 23 (for the P25  $\text{TiO}_2$ -based cell) and 49% (for the aerogel-based cell) more than that of the P25  $\text{TiO}_2$ -based cell. The end results were a larger efficiency improvement of 1.17% (from 7.19 to 8.36%) for the aerogel-based cell as compared to 0.9% (from 6.32 to 7.22%) for the P25  $\text{TiO}_2$ -based cell.

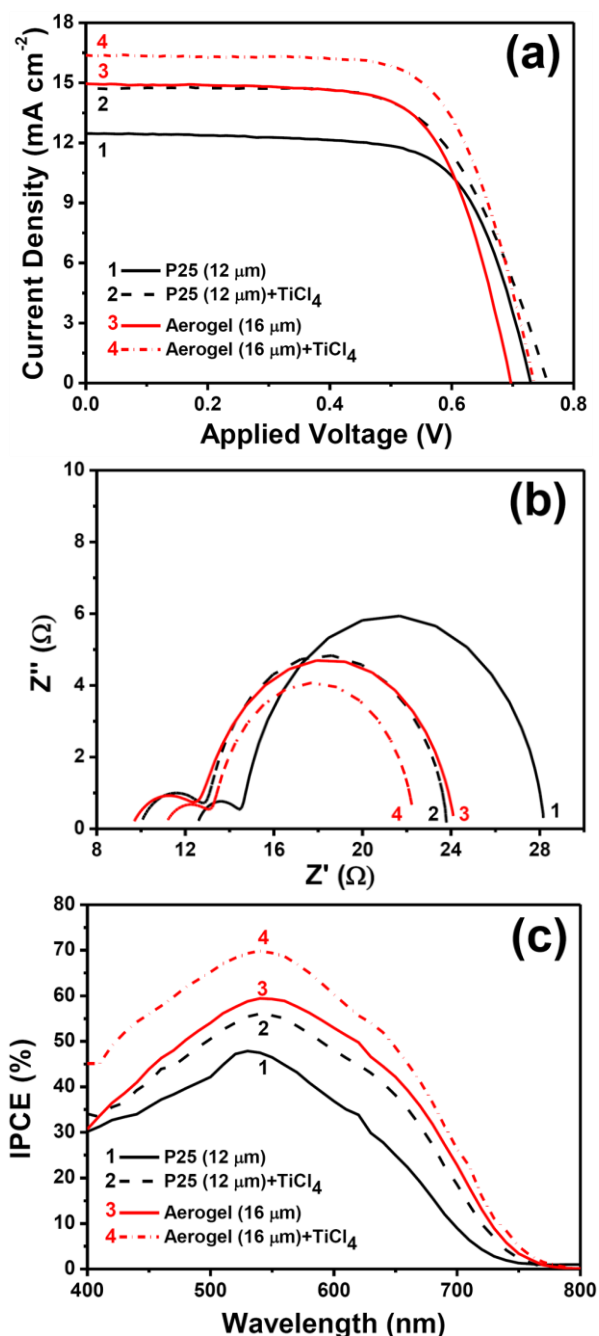


**Figure 3.** (a) Current density vs. applied voltage plot, (b) Nyquist plot, and (c) IPCE curves of aerogel and P25  $\text{TiO}_2$ -based cells at optimum photoanode thicknesses.

Figure 3(c) shows the IPCE curves for the four cells. The superiority of the  $\text{TiO}_2$  aerogel over P25  $\text{TiO}_2$  as the photoanode material was again verified by the consistently higher IPCE of the

aerogel-based cell across the entire wavelength range. Also evident is the lift in IPCE achieved with the  $\text{TiCl}_4$  treatment. The electron life times were also determined from the intensity-modulated photovoltage spectroscopy [27] for the P25 and aerogel samples at a thickness of 12  $\mu\text{m}$  under a light intensity of 30  $\text{mW cm}^{-2}$ , to be 199 and 398 ms, respectively. The much longer electron life time of the aerogel anode may be attributed to its well-connected 3D network for better de-localization of the diffusing electrons. Longer electron life times mean better chances for the electrons to make it to the current collector instead of being consumed during the diffusion across the photoanode layer, thus are advantageous for achieving higher power conversion efficiencies.

#### 4. CONCLUSION

In conclusion,  $\text{TiO}_2$  aerogels were prepared and demonstrated a superior mesoporous structure for the fabrication of the photoanodes of DSSCs than P25 nanoparticles. A 16% improvement in the power conversion efficiency was realized with the  $\text{TiO}_2$  aerogel-based cell over the P25  $\text{TiO}_2$ -based one. The success was attributed to the structural advantages of the  $\text{TiO}_2$  aerogel, including high specific surface areas, high porosities, and three-dimensionally well-connected through pore structure.

#### ACKNOWLEDGMENTS

This work was financially supported by the National Science Council of the Republic of China (Taiwan) under grants NSC-98-2221-E-036-MY3 and NSC-98-3114-E-007-005 and by the Low Carbon Energy Research Center of the National Tsing-Hua University.

#### References

1. C. Pierre and G. M. Pajonk, *Chem. Rev.*, 102 (2002) 4243
2. T. Y. Wei, T. F. Cheng, S. Y. Lu and Y. C. Chang, *J. Am. Ceram. Soc.*, 90 (2007) 2003
3. G. S. Kim and S. H. Hyun, *Thin Solid Films*, 460 (2004) 190
4. T. Y. Wei, S. Y. Lu and Y. C. Chang, *J. Phys. Chem. B*, 112 (2008) 11881
5. T. Y. Wei, S. Y. Lu and Y. C. Chang, *J. Phys. Chem. C*, 113 (2009) 7424
6. T. Y. Wei, C. H. Chen, K. H. Chang, S. Y. Lu and C. C. Hu, *Chem. Mater.*, 21 (2009) 3228
7. T. Y. Wei, C. H. Chen, H. C. Chien, S. Y. Lu and C. C. Hu, *Adv. Mater.*, 22 (2010) 347
8. C. C. Lin, T. Y. Wei, K. T. Lee and S. Y. Lu, *J. Mater. Chem.*, 21 (2011) 12668
9. Y. H. Lin, T. Y. Wei, H. C. Chien and S. Y. Lu, *Adv. Energy Mater.*, 1 (2011) 901
10. H. C. Chien, W. Y. Cheng, Y. H. Wang, T. Y. Wei and S. Y. Lu, *J. Mater. Chem.*, 21 (2011) 18180
11. M. Gratzel, *Accounts Chem. Res.*, 42 (2009) 1788
12. M. K. Nazeeruddin, E. Baranoff and M. Gratzel, *Sol. Energy*, 85 (2011) 1172
13. Y. Kuo and S. Y. Lu, *Nanotechnology*, 19 (2008) 095705
14. T. Y. Tsai and S. Y. Lu, *Electrochem. Commun.*, 11 (2009) 2180
15. T. Hsiao, S. Y. Lu and T. Y. Tsai, *Chem.-A Eur. J.*, 17 (2011) 1358
16. T. Y. Tsai and S. Y. Lu, *J. Electrochem. Soc.*, 158 (2011) B1306
17. S. Y. Ku and S. Y. Lu, *Int. J. Electrochem. Sci.*, 6 (2011) 5219
18. M.-S. Wu and Y.-J. Zheng, *Int. J. Electrochem. Sci.*, 7 (2012) 1187
19. Z. Wei, Y. Yao, T. Huang and A. S. Yu, *Int. J. Electrochem. Sci.*, 6 (2011) 1871

20. T.-H. Tsai, S.-C. Chiou and S.-M. Chen, *Int. J. Electrochem. Sci.*, 6 (2011) 3333
21. J. J. Pietron, A. M. Stux, R. S. Compton and D. R. Rolison, *Sol. Energy Mater. Sol. Cells*, 91 (2007) 1066
22. W. J. Sung, S. H. Hyun, D. H. Kim, D. S. Kim and J. Ryu, *J. Mater. Sci.*, 44 (2009) 3997
23. G. Dagan and M. Tomkiewicz, *J. Phys. Chem.*, 97 (1993) 12651
24. S. R. Gajjela, K. Ananthanarayanan, C. Yap, M. Gratzel and P. Balaya, *Energy Environ. Sci.*, 3 (2010) 838
25. T.-S., Kang, S.-H. Moon and K.-J. Kim, *J. Electrochem. Soc.*, 149 (2002) E155
26. M. Adachi, M. Sakamoto, J. Jiu, Y. Ogata and S. Isoda, *J. Phys. Chem. B*, 110 (2006) 13872
27. J. Kruger, R. Plass, M. Gratzel, P. J. Cameron and L. M. Peter, *J. Phys. Chem. B*, 107 (2003) 7536